

CLIMATOLOGY OF THE VERTICAL PROFILES OF POLARIMETRIC RADAR VARIABLES AT X BAND IN STRATIFORM CLOUDS

5

Silke Trömel¹, Alexander V. Ryzhkov², Brandon Hickman¹, Clemens Simmer¹

¹Meteorological Institute, University of Bonn, Germany

²Cooperative Institute for Mesoscale Meteorological Studies, University of Oklahoma, Norman, Oklahoma, and NOAA/OAR/National Severe Storms Laboratory, Norman, Oklahoma

1. INTRODUCTION

Quasi-Vertical Profiles (QVPs) of polarimetric variables emerged as a simple but effective way to process and display radar data. Quasi-Vertical Profiles (QVP) were first used by Kumjian et al. (2013) to identify polarimetric signatures of refreezing in winter storms and by Trömel et al. (2014) to reliably estimate backscatter differential phase δ within the melting layer. Ryzhkov et al. (2016) further expanded the QVP methodology and demonstrated its multiple benefits. QVPs are obtained via azimuthal averaging of PPIs measured at an elevation angle between 10 and 20 deg in order to take advantage of the polarimetric signals, which decrease only slightly with increasing elevation if the elevation angle remains below this angle range. The slant range coordinate is transformed into height above ground, and the resulting QVPs are presented in a height versus time display (Fig. 1). The statistical noise reduction as a result of the azimuthal averaging process enables us to better detect and quantify signatures in the melting layer (ML) and the dendritic growth layer (DGL), which are often noisy and hard to quantify in standard conical PPIs or RHIs. Another advantage of QVPs is a relatively high vertical resolution, which is about 30 m in Fig. 1 using the 18° elevation scan measured by the polarimetric X band radar in Bonn, Germany, (BoXPol, for details of the radar see Diederich et al., 2015a, b) with a radial resolution of 100 m.

Statistics of QVPs for 52 stratiform events observed with BoXPol for periods between 1h 20 min and 12h 30min have been estimated motivated by three major applications

- The generation of look-up tables characterizing the intrinsic vertical profiles of reflectivity Z_H needed for the implementation of a polarimetric VPR (vertical profile of reflectivity) technique
- The reliable estimation of polarimetric variables in the DGL for nowcasting applications with a focus on gradients in reflectivity Z_H and enhanced specific differential phase K_{DP}
- The reliable estimation of polarimetric variables in the ML in order to evaluate the

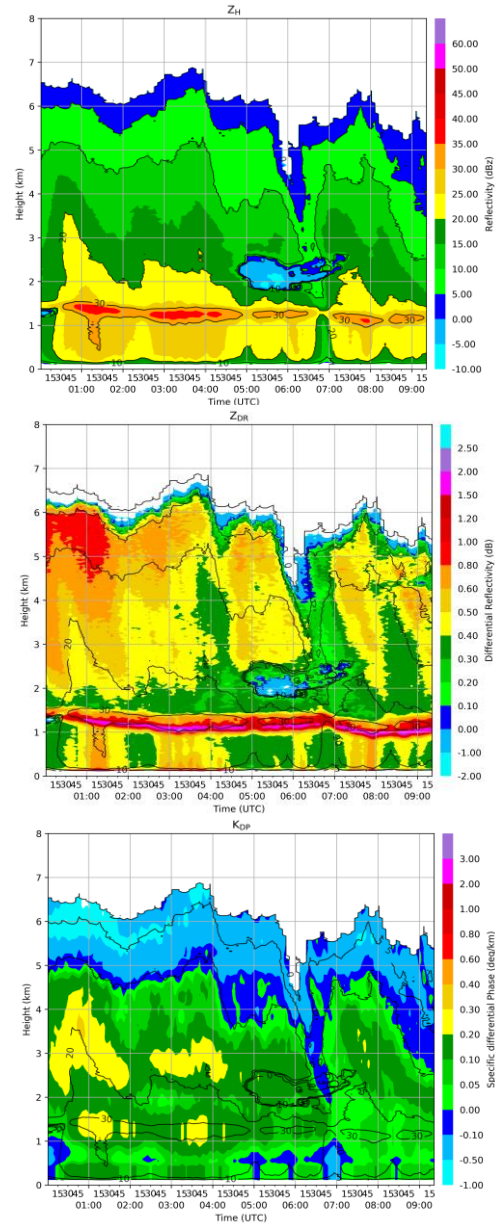


Figure 1: Quasi-vertical profiles (QVPs) of Z_H (top), Z_{DR} (middle) and K_{DP} (bottom) with black Z_H contour lines observed with the BoXPol radar in Bonn, Germany, at 18° elevation on 16 November 2014 between 0:00 and 9:25 UTC.

representation of clouds and precipitation microphysical processes in numerical models.

The following three sections give a short overview of results within these research areas, i.e., Section 2 introduces the polarimetric VPR technique, Section 3 describes the envisioned observation-based nowcasting technique exploiting the signatures in the DGL, and Section 4 summarizes the statistics of polarimetric variables in the ML at X band. Finally, Section 5 briefly presents the major conclusions.

2. POLARIMETRIC VPR TECHNIQUE

The mitigation of brightband contamination and the exploitation of observations of frozen hydrometeors above the brightband for surface rain rate estimates in the framework of VPR techniques require a reliable detection and quantification of the brightband. We use the statistics of the 52 stratiform events to derive look-up tables of the apparent profiles of radar reflectivity for the following 6 parameters of the intrinsic profiles of Z_H : maximal value of Z_H within the ML (Z_{peak}), Z_H in rain below the melting layer (Z_{rain}), Z_H of frozen hydrometeors just above the melting layer (Z_{snow}), the vertical gradient of Z_H above the melting layer (β), the melting layer top height (ML_{top}), and the melting

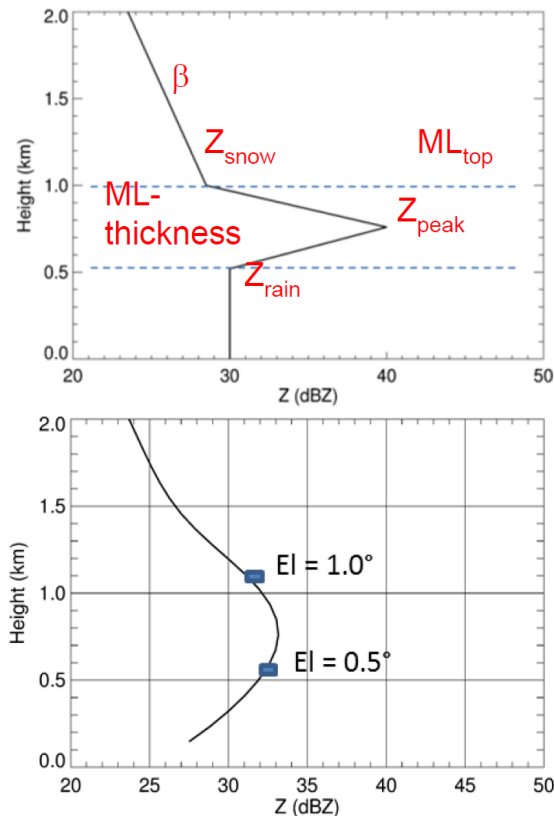


Figure 2: Schematic of an intrinsic vertical profile of Z_H characterized by 6 parameters (top) and the respective apparent/measured Z_H values at a distance of 50 km at elevation 0.5° and 1.0° (blue points, bottom) assuming a 1° antenna beam width.

layer depth (ML-thickness; see top panel of Fig. 2). Given the respective profiles based on the derived 6 parameters, they can be transformed into apparent/measured profiles at any distance from the radar if its antenna pattern is known. The bottom panel of Figure 2 shows such a reconstructed profile, which clearly demonstrates the smoothing effects due to the beam broadening and its difference from the intrinsic profile must be taken into account before any interpretation. E.g. at 0.5° elevation the measured Z_H at a distance of 50 km is 32.5 dBZ and thus 2.5 dB above the true (intrinsic) value, which should be used for the surface precipitation estimation. Consequently, 2.5 dB has to be subtracted from the measured Z_H before the application of rainfall retrievals.

The study of Fabry and Zawadzki (1995) is still the most cited reference concerning melting layer statistics, which does, however, not yet include

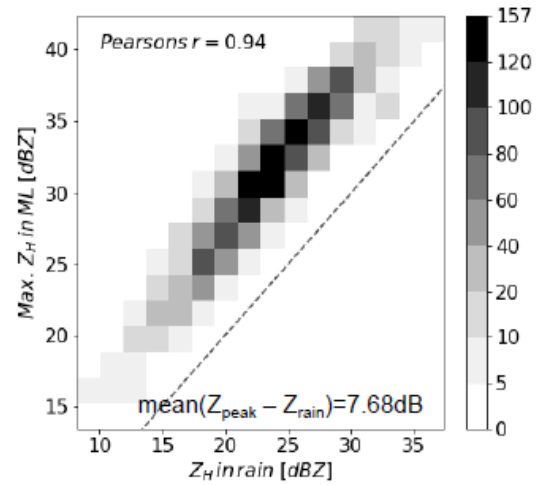


Figure 3: Scatter density plot based on 52 events comparing the peak reflectivity Z_{peak} with the reflectivity in rain Z_{rain} just below the ML.

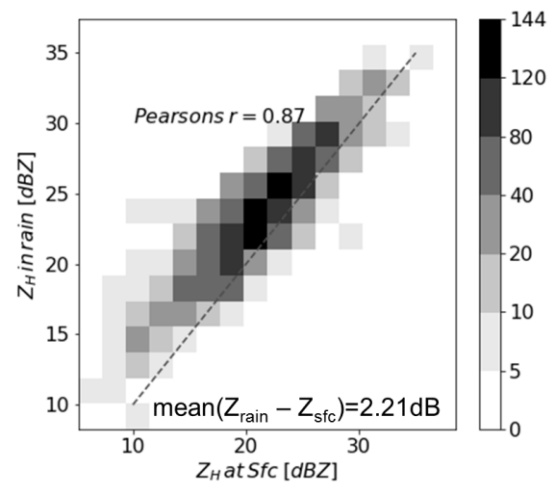


Figure 4: Scatter density plot based on 52 events comparing the reflectivity in rain Z_{rain} with the reflectivity near the surface Z_{sfc} .

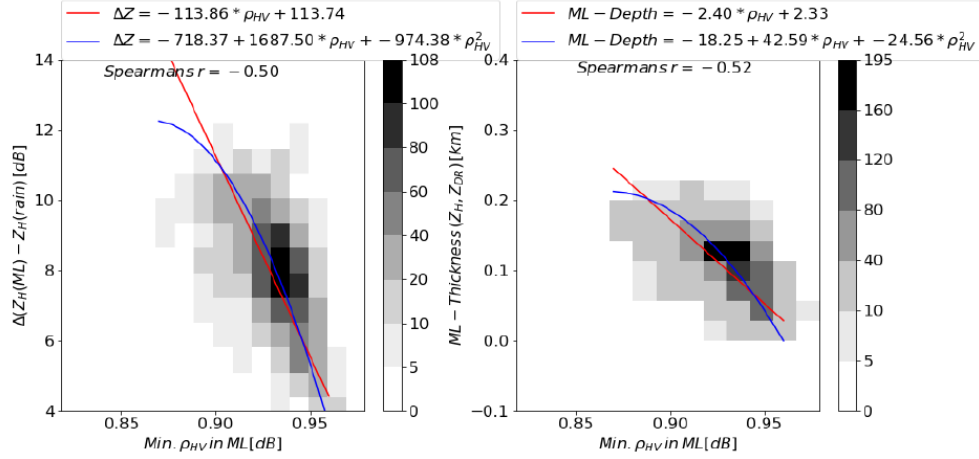


Figure 5: Scatter density plots based on 52 events comparing $(Z_{\text{peak}} - Z_{\text{rain}})$ with the minimum of ρ_{HV} in the ML (left), and the difference in the heights of the Z_{H} and Z_{DR} maxima (proportional to ML-depth) with the minimum ML ρ_{HV} (right). Red and blue lines indicate the corresponding linear and polynomial fits of order 2, respectively.

polarimetric information. The study analyzed 600 hours of vertically pointing X-band radar data collected at the Marshall Observatory radar site in Canada. According to their statistics, the difference between the ML reflectivity peak, Z_{peak} , and the reflectivity in rain, Z_{rain} , just below the ML varies between 5 and 12 dB with increasing difference above 19 dBZ of Z_{rain} .

Our analysis of the BoXPOL observations for the 52 stratiform events result in an average difference $Z_{\text{peak}} - Z_{\text{rain}}$ of 7.7 dB with a standard deviation of 1.9 dB, but no significant change/increase at higher dBZ values is discernable. Fabry and Zawadzki (1995) assume no change in Z_{rain} below the ML while we see an average decrease of Z_{H} equal to 2.2 dB with a standard deviation of 2.7 dB in an average rain layer depth of 1.9 km likely attributed to evaporation (Fig. 4). Besides relative humidity also the droplet size, as indicated by the differential reflectivity Z_{DR} (low Z_{DR} indicates small droplets which evaporate faster) influences evaporation intensity. A potential dominance of smaller drops in stratiform rain in Germany may be the reason for the difference between the statistics. For relative humidity $\text{RH}=60\%$ and $Z_{\text{DR}}=0.27$ dB the expected reflectivity reduction within a 2 km deep rain layer (average rain layer depth in BoXPOL observations is 1.9 km with a standard deviation of 0.78 km) ranges between 2 and 5 dB (Kumjian and Ryzhkov 2010, Xie et al. 2015).

In this study we extend the statistics by Fabry and Zawadzki (1995) by correlations among the polarimetric variables to further reduce the uncertainty of the respective intrinsic profile. The right panel of Fig. 5 shows the difference between the heights of the Z_{H} and Z_{DR} maxima, which is proportional to ML-thickness, against the minimum values of the cross-correlation coefficient ρ_{HV} in the ML. On the left panel, the difference between the reflectivity peak value and the reflectivity in rain is

plotted versus the minimum ρ_{HV} in the ML. Smaller ρ_{HV} points to bigger differences in the mentioned reflectivity values.

We can conclude that, if ρ_{HV} is low we have to search for lookup table entries at deeper ML and higher $\Delta Z = (Z_{\text{peak}} - Z_{\text{rain}})$ values. Since ρ_{HV} correlates well with ΔZ and ML-thickness (see Fig. 4), one should pick a Z_{H} -profile based on ρ_{HV} by making use of the correlations indicated at the top of Fig. 4 and estimate the bias of Z_{H} attributed to the brightband contamination at every distance from the radar.

At larger distances from the radar, the range dependency of Z_{H} is determined by the slope β (Fig. 2) of the reflectivity profile above the ML. β and the corresponding negative bias of Z_{H} can be obtained from the difference of Z_{H} at two successive antenna elevations (e.g., 0.5 deg and 1.0 deg).

3. EXPLOITING SIGNATURES IN THE DGL FOR NOWCASTING

Pristine crystals are in most cases generated near the top of the clouds from where they grow while falling by deposition, aggregation, or riming. Kennedy and Rutledge (2011) first described the polarimetric signature of dendritic growth as a band of high K_{DP} in an area of low ρ_{HV} and enhanced vertical gradient of Z_{H} near the -15°C environmental temperature level; they also pointed to increased precipitation intensity beneath such layers. Dendritic growth, however, has also been found to produce a band of enhanced Z_{DR} (Andrić et al. 2013; Williams et al. 2015), while aggregation and riming tends to reduce Z_{DR} due to decreasing bulk density and/or oblateness. Hence, Z_{H} increases, Z_{DR} decreases, and ρ_{HV} increases below the DGL towards the ground. The signatures in the DGL, more broadly defined as the height levels located between -10 and -15°C , have high potential for observation-

based nowcasting. Assuming a DGL of about 2 km above the ML and a fall velocity of 1m/s for snowflakes, we can expect 30 minutes and more of lead time compared to its signal in surface precipitation. The QVP technique enables us to better quantify these valuable signatures, which are often noisy in PPI scans or reconstructed RHIs. Fig. 1 shows the bands of enhanced Z_{DR} and K_{DP} aloft indicating the DGL. K_{DP} bands indicate an increased number concentration of ice crystals, that leads to aggregation and masking of Z_{DR} bands (Moisseev et al. 2015). Thus, the pronounced K_{DP} bands in the first half of the observation period also indicate higher precipitation intensities, which is confirmed by rain gauge measurements located in the vicinity of BoXPoI for the case presented in Fig.1. Fig. 6 shows the temporal evolution of Z_H , K_{DP} , and Z_{DR} in the DGL for the same event, defined as the 95th percentiles of the azimuthally averaged variables within the layer between -10°C and -15°C presented in Fig.1. Lagged correlations show a

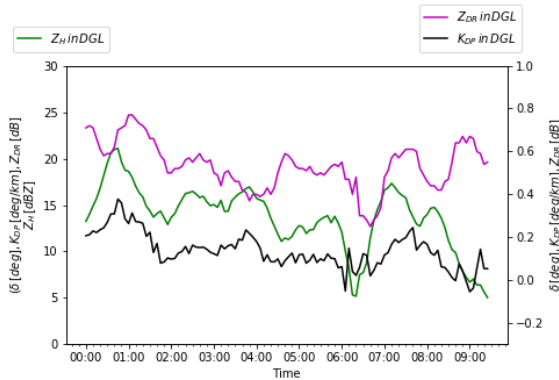


Figure 6: Temporal evolution for Z_H (green), K_{DP} (black), and Z_{DR} (purple) in the DGL for 16 November 2014 defined as the respective 95th percentile of azimuthal averaged QVPs in the temperature range between -10°C and -15°C (compare Fig. 1).

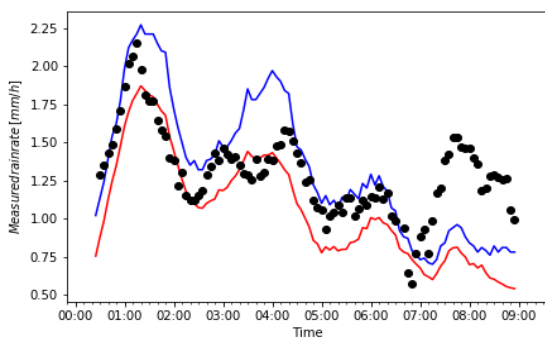


Figure 7: Mean measured hourly rain rates for the event observed on 16 November 2014 based on 2 (blue line) and 5 (red line) rain gauges close to BoXPoI together with the fitted rain retrieval $R(Z_H, K_{DP})$ exploiting the signatures in the DGL (black dots) taking 30 min. lag time into account.

maximum Pearson correlation coefficient $r=0.86$ between the time series of Z_H in the DGL and Z_H near the surface for a lag time of 30 min., i.e. maximal values in the DGL precede precipitation enhancements near the surface by the approximate time needed for snowflakes generated aloft to reach the ground.

Fitting Z_H and K_{DP} in the DGL to the 30 min. lagged average hourly rain rate near the surface based on two rain gauges close to the radar results in the nowcasting retrieval

$$R(Z_H, K_{DP}) = 0.86 K_{DP}^{0.18} Z_H^{0.22}. \quad (1)$$

Fig. 7 shows the overall agreement of derived rain rates using Eq. 1 with observations from rain gauges. The findings are in line with past studies suggesting that water mass fluxes just above the freezing level and below the ML do not differ much (Ohtake 1969, Barthazy et al. 1998, Zhang et al. 2011, Heymsfield and Matrosov 2016), hence the snow liquid equivalent rate S and rain rate near the surface R are close to each other if evaporation is not significant.

The time lag between K_{DP} enhancement aloft and the intensification of rain at the surface shows the value of the signatures in the DGL for nowcasting. Of course, one has to take into account the trajectories of snowflakes forming aloft in order to predict locations of snow enhancement at the surface which involves the analysis of horizontal wind. The inspection of the performance of the numerical weather prediction model COSMO-DE (Doms and Schättler 2002, Baldauf et al. 2011) for this event show relatively weak horizontal winds mostly below 10m/s up to the -15°C level during this event. Thus snowflakes mostly stayed within the QVP cone of azimuthal averaging. For higher winds, snowflakes may be advected out of the cone and the correlation between DGL signatures in the QVP profiles and the surface precipitation rate might be reduced as found in a number of examined cases.

In the envisioned nowcasting strategy, one should first detect strong signals in the DGL in terms of large Z_H gradients, i.e. β (see Fig. 2, top panel), and high K_{DP} . Using the wind information from NWP or radars the trajectories of snow generated aloft towards the surface can be calculated. Climatological vertical profiles of snow liquid equivalent rates S are required to project the measurements in the DGL to the surface.

4. POLARIMETRIC VARIABLES IN THE ML AT X BAND

The polarimetric signatures in the ML provide insights into the microphysical processes both within and above the ML. Still, the most sophisticated cloud models are not able to adequately reproduce vertical profiles of polarimetric radar variables within the ML. Further improvements require first of all solid statistics concerning the comparison between observed and simulated radar variables.

An analysis of the ML using range height indicator (RHI) scans was carried out by Wolfensberger et al. (2015) with the focus on Z_H and ρ_{HV} . In our analyses, we use the detection methodology of Hickman et al. (2017), which largely follows Wolfensberger et al. (2015) but uses QVPs as data base. Following Trömel et al. (2014) and Griffin et al. (2017) for separating K_{DP} and backscatter differential phase δ in the QVP profiles of total differential phase, quite robust estimates of K_{DP} within the ML have been obtained for the first time. K_{DP} is a very valuable ML parameter because it better characterizes precipitation flux within the ML than Z_H and differential reflectivity Z_{DR} , both heavily weighted by large wet snow aggregates.

A reliable statistics of K_{DP} in the DGL and ML are essential to improve microphysical parameterizations in existing NWP models, which tend to overestimate the size and underestimate the concentration of ice and snow in stratiform clouds (e.g., Fridlind et al. 2017). High values of K_{DP} are indicative of high concentrations of primary ice nucleated at the tops of the clouds (Griffin et al. 2017). Fig. 8 presents the histograms of observed polarimetric variables in the ML and the slope β

(see Fig. 2) in the reflectivity profile above the ML at X band as derived from the 52 stratiform events investigated. Backscatter differential phase δ at X band in the ML varies between 0.1 and 5 deg. K_{DP} in the ML is on average around 0.61 deg/km, maximal values reach 2.85 deg/km. As indicated by the histogram of β , Z_H decreases with height at the average rate of about 4 dB/km, which is in line with previous publications (Fabry and Zawadzki 1995, Steiner et al. 1995, Vignal and Krajewski 2001, Bellon et al. 2005, Matrosov et al. 2009).

5. SUMMARY AND OUTLOOK

Statistics based on 52 stratiform events in Germany observed with the polarimetric X band radar in Bonn (BoXPoI) have been analyzed. Due to the high vertical resolution and inherent reduction of statistical noise, the QVP method allows a reliable estimation of intrinsic polarimetric profiles of the melting layer and the dendritic growth layer, mandatory for the development of a polarimetric VPR technique and for exploiting the valuable radar signatures in the DGL for nowcasting. Moreover, the high precision of the thus derived polarimetric radar variables might allow for deeper insights in the microphysics within and above the ML. However, it has to be mentioned that our statistics do not include a wide range of rain rates. In Bonn, Germany, the stratiform cases are mostly associated with relatively low rain rates. The cases investigated include a mean rain rate of only 1.3 mm/h.

The proposed polarimetric VPR method allows one to pick appropriate intrinsic profiles of Z_H from a lookup table depending on (1) the height of the ML,

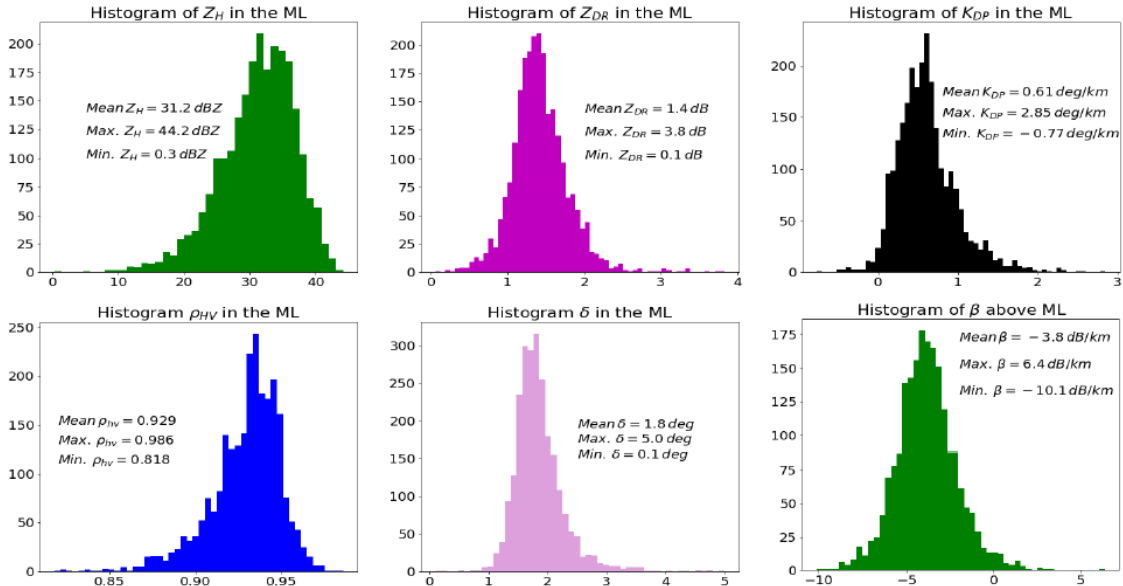


Figure 8: Histograms of the polarimetric variables in the ML and the slope β above the ML at X band based on 52 stratiform events analyzed in terms of QVPs.

and (2) the observed Z_H , Z_{DR} , and ρ_{HV} . At longer distances, the range dependency of Z_H is determined by the slope β .

The use of Z_H and K_{DP} in the DGL is promising for nowcasting precipitation estimation including tendencies (Fig. 7), but trajectories to the surface using wind information have to be calculated under strong wind conditions. Due to the azimuthal averaging of radar data at higher elevations, the QVPs have different horizontal resolutions in the DGL and closer the surface. The Columnar Vertical Profile Methodology (CVPs) suggested by Murphy et al. (2017) has a good chance to overcome some deficiencies of the QVP technique. Whereas QVPs average radar data over the full range and azimuth of one radar elevation scan, CVPs average data within a prescribed sector in range and azimuth and over multiple radar elevation tilts. Thus QVPs are radar-centric while CVPs can be calculated at any location within the radar range. Hence the proposed nowcasting strategy includes the detection of respective signatures in the DGL using CVPs and the calculation of the trajectories of hydrometeors to the surface utilizing wind information.

The combination of the QVP-methodology with a melting-layer detection strategy allowed to reliably estimate Z_H , Z_{DR} , and ρ_{HV} and also to separate K_{DP} and δ in the ML. Confidence in the δ - K_{DP} -decomposition is supported by a high correlation between K_{DP} in the ML and measured rain rate at the surface ($r=0.56$), as well as high correlation between K_{DP} in the ML and Z_{peak} ($r=0.58$) and also high correlation between maximal Z_{DR} in the ML and δ in the ML.

We believe that the utilization of the K_{DP} measurements in the DGL and ML would help the modelers to refine their microphysical parameterization schemes. K_{DP} is a lower moment of snow size distribution than Z_H and its use is essential for better understanding and quantification of the microphysical processes involving ice and snow.

6. REFERENCES

- Andrić, J., M. R. Kumjian, D. Zrnić, J. M. Straka, and V. M. Melnikov, 2013: Polarimetric signatures above the melting layer in winter storms: An observational and modeling study. *J. Appl. Meteor. Climatol.*, 52, 682–700, doi:10.1175/JAMC-D-12-028.1.
- Baldauf, M., A. Seifert, J. Förstner, D. Majewski, M. Raschendorfer, T. Reinhardt, 2011: Operational convective-scale numerical weather prediction with the COSMO model: Description and sensitivities. *Mon. Weather Rev.* 139:3887–3905, doi:10.1175/MWR-D-10-05013.1.
- Barthazy, E., W. Henrich, A. Waldvogel, 1998: Size distribution of hydrometeors through the melting layer. *Atmos. Research*, 47 – 48, 193 – 208.
- Bellon, A., G. Lee, and I. Zawadzki, 2005: Error statistics of VPR corrections in stratiform precipitation. *J. Appl. Meteor.*, 44, 998 – 1015.
- Diederich, M., A. Ryzhkov, C. Simmer, P. Zhang, and S. Trömel, 2015a: Use of specific attenuation for rainfall measurement at X-band radar wavelengths - Part 1: Radar calibration and partial beam blockage estimation. *Journal of Hydrometeorology*, 16, 2, 487-502, doi:10.1175/JHM-D-14-0066.1
- Diederich, M., A. Ryzhkov, C. Simmer, P. Zhang, and S. Trömel, 2015b: Use of specific attenuation for rainfall measurement at X-band radar wavelengths - Part 2: Rainfall estimates and comparison with rain gauges. *Journal of Hydrometeorology*, 16, 2, 503-516, doi:10.1175/JHM-D-14-0067.1
- Doms, G., and U. Schättler, 2002: A description of the non-hydrostatic regional model LM, Part I: Dynamics and numerics. *COSMO Newsl. 2*: 225–235.
- Fabry, F., and I. Zawadzki, 1995: Long-term radar observations of the melting layer of precipitation and their interpretation. *J. Atmos. Sci.*, 52, 838 – 851.
- Fridlind, A. M., X. Li, D. Wu, M. van Lier-Walqui, A.S. Ackerman, W.-K. Tao, G.M. McFarquhar, W. Wu, X. Dong, J. Wang, A. Ryzhkov, P. Zhang, M.R. Poellot, A. Neumann, and J.M. Tomlinson, 2017: Derivation of aerosol profiles for MC3E convection studies and use in simulations of the 20 May squall line case. *Atmos. Chem. Phys.*, 17, 5947-5972, doi:10.5194/acp-17-5947-2017.
- Griffin, E., T. Schuur, and A. Ryzhkov, 2017: A polarimetric analysis of ice microphysical processes in snow using quasi-vertical profiles. *J. Appl. Meteorol. Clim.*, in review.
- Heymsfield, A., and S. Matrosov, 2016: Toward improving ice water content and snow-rate retrievals from radars. Part I: X and W bands, emphasizing CloudSat. *J. Appl. Meteorol. Clim.*, 55, 2063 – 2089.
- Hickman, B. S., S. Trömel, A.V. Ryzhkov, and C. Simmer 2017: Radar-Driven Temperature Nudging for Nowcasting Winter Precipitation. Extended Abstract, 38th Conference on Radar Meteorology, 28 August -1 September 2017, Chicago, Illinois, USA

- Kennedy, P. C., and S. A. Rutledge, 2011: S-band dual-polarization radar observations of winter storms. *J. Appl. Meteor. Climatol.* 50, 844–858, doi:10.1175/2010JAMC2558.1.
- Kumjian, M.R. and A.V. Ryzhkov, 2010: The impact of evaporation on polarimetric characteristics of rain: Theoretical model and practical implications. *J. Appl. Meteor. Climatol.*, 49, 1247-1267.
- Kumjian, M.R., A.V. Ryzhkov, H.D. Reeves, and T.J. Schuur, 2013: A dual-polarization radar signature of hydrometeor refreezing in winter storms. *J. Appl. Meteor. Climatol.*, 52, 2549-2566.
- Matrosov, S., C. Campbell, D. Kingsmill, and E. Sukovich, 2009: Assessing snowfall rates from X-band radar reflectivity measurements. *J. Atmos. Oceanic Technol.*, 26, 2324 – 2339.
- Moisseev, D. N., S. Lautaportti, J. Tyynela, and S. Lim, 2015: Dualpolarization radar signatures in snowstorms: Role of snowflake aggregation. *J. Geophys. Res. Atmos.*, 120, 12 644–12 655, doi:10.1002/2015JD023884.
- Murphy, A., A. Ryzhkov, P. Zhang, G. McFarquhar, W. Wu, and D. Stechman, 2017: A Polarimetric and Microphysical Analysis of the Stratiform Rain Region of MCSs. Presentation #88, 38th Conference on Radar Meteorology, 28 August -1 September 2017, Chicago, Illinois, USA.
- Ohtake, T., 1969: Observations of Size Distributions of Hydrometeors Through the Melting Layer. *J. Atmos. Sci.*, 26, 545–557, doi: 10.1175/1520-0469(1969)026<0545:OOSDOH>2.0.CO;2
- Ryzhkov, A., P. Zhang, H. Reeves, M. Kumjian, T. Tschallener, S. Trömel, and C. Simmer, 2016: Quasi-vertical profiles – a new way to look at polarimetric radar data. *J. Atmos. Oceanic Technol.* 33, 551-562. DOI: 10.1175/JTECH-D-15-0020.1
- Steiner, M., R. Houze, and S. Yuter, 1995: Climatological characterization of three-dimensional storm structure from operational radar and rain gauge data. *J. Appl. Meteor.*, 34, 1978 – 2007.
- Trömel, S., A. Ryzhkov, P. Zhang, C. Simmer, 2014: Investigations of backscatter differential phase in the melting layer. *J. Appl. Met. Clim.*, 53(10), 2344-2359, doi: 10.1175/JAMC-D-14-0050.1
- Vignal, B., and W. Krajewski, 2001: Large-sample evaluation of two methods to correct range-dependent error for WSR-88D rainfall estimates. *J. Hydrometeorol.*, 2, 490 – 504.
- Williams, E., D. Smalley, M. Donovan, R. Hollowell, K. Hood, B. Bennett, R. Evaristo, A. Stepanek, T. Bals-Elsholz, J. Cobb, J. Ritzman, A. Korolev, and M. Wolde, 2015: Measurements of Differential Reflectivity in Snowstorms and Warm Season Stratiform Systems. *J. Appl. Meteor. Climatol.*, 54, 573–595,
- Wolfensberger, D., D. Scipion, A. Berne, 2015: Detection and characterization of the melting layer based on polarimetric radar scans. *Q.J.R. Meteorol. Solc.* doi:10.1002/qj.2672
- Zhang, G., S. Luchs, A. Ryzhkov, M. Xue, L. Ryzhkova, and Q. Cao, 2011: Winter Precipitation Microphysics Characterized by Polarimetric Radar and Video Disdrometer Observations in Central Oklahoma. *J. Appl. Meteor. Climatol.*, 50, 1558–1570
- Xie, X., R. Evaristo, S. Trömel, P. Saavedra, C. Simmer, A. Ryzhkov, 2015: Radar Observation of Evaporation and Implications for Quantitative Precipitation and Cooling Rate Estimation. *J. Atmos. Oceanic Technol.* 33(8), 1779-1792, doi: 10.1175/JTECH-D-15-0244.1